Subduction history reveals Cretaceous slab superflux as a possible cause for the mid-Cretaceous plume pulse and superswell events

Madison East[1*], R Dietmar Müller[1], Simon Williams[1], Sabin Zahirovic[1] and Christian Heine[2]

[1] EarthByte Group, School of Geosciences, University of Sydney, Sydney, New South Wales 2006, Australia.
[2] Specialist Geosciences (PTD/E/F), Projects & Technology, Shell Global Solutions International B.V., Rijswijk, The Netherlands.
[*] Corresponding author. Email: meas7937@uni.sydney.edu.au

Key words: subduction; slab flux; tectonics; Cretaceous; superswell

Research Highlights:

- Complete model of slab flux and subducting plate area since the Late Triassic
- Cretaceous slab superflux event revealed following Pangea break-up
- A trigger for the mid-Cretaceous plume pulse and superswell events?

This manuscript is a non-peer reviewed preprint submitted to EarthArXiv. It has been submitted to the journal Gondwana Research and conditionally accepted.

Abstract

Subduction is a fundamental mechanism of material exchange between the planetary interior and the surface. Despite its significance, our current understanding of fluctuating subducting plate area and slab volume flux has been limited to a range of proxy estimates. Here we present a new detailed quantification of subduction zone parameters from the Late Triassic to present day (230 – 0 Ma). We use a community plate motion model with evolving plate topologies to extract trench-normal convergence rates through time to compute subducting plate areas, and we use seafloor paleo-age grids to estimate the thickness of subducting lithosphere to derive the slab flux through time. Our results imply that slab flux doubled to values greater than 500 km^3/yr from 180 Ma in the Jurassic to 130 Ma in the mid-Cretaceous, subsequently halving again towards the Cretaceous-Paleogene boundary, largely driven by subduction zones rimming the Pacific ocean basin. The 130 Ma spike can be attributed to a two-fold increase in mid-ocean ridge lengths following the break-up of Pangea, and a coincident increase in convergence rates, with average speeds exceeding 10 cm/yr. With one third of the total 230 - 0 Ma subducted volume entering the mantle during this short ~ 50 Myr period, we suggest this slab superflux drove a surge in slab penetration into the lower mantle and an associated increase in the vigour of mantle return flow. This mid-Cretaceous event may have triggered, or at least contributed to, the formation of the Darwin Rise mantle superswell, dynamic elevation of the South African Plateau and the plume pulse that produced the Ontong-Java-Hikurangi-Manihiki and Kerguelen plateaus, among others.

The models presented here contribute to an improved understanding of the time-evolving flux of material consumed by subduction, and suggest that slab superflux may be a general feature of continental dispersal following supercontinent breakup. These insights may be useful for better understanding how supercontinent cycles are related to transient episodes of large igneous province and superswell formation, and the associated deep cycling of minerals and volatiles, as well as leading to a better understanding of tectonic drivers of long-term climate and icehouse-to-greenhouse transitions.

1 Introduction

Estimating how subduction has changed through time on a global scale is key to better understanding the evolution of a range of Earth processes. As a crucial driving forces in plate tectonics, subduction zones can alter ocean basin configurations and plate trajectories. In addition, subduction plays a role in the carbonate-silicate cycle and atmospheric CO_2 concentrations (Bergman et al., 2004, Müller and Dutkiewicz, 2018) through degassing from arc volcanism. Subducted slabs can also influence the nature of mantle convection and mantle composition, acting as a perturbation to the planet's internal dynamics (Zhong and Rudolph, 2015, Hofmann, 1997).

Most of our understanding of subduction over geological timescales has come from estimates and proxies of subducting seafloor area at convergent margins. This has been achieved using methods of long-term sea level inversion (Gaffin, 1987), detailed plate reconstruction models (Coltice et al., 2013, Engebretson et al., 1992) and seismic tomographic imaging (Shephard et al., 2017). However, the volume of slab material being consumed at subduction zones (slab flux) has received less attention, with the exception of the study by Wen and Anderson (1995). While estimates of subducted seafloor area have played an important role in carbon and geochemical modelling (Berner, 1994, Bergman et al., 2004), knowledge of the subducted lithospheric volume as opposed to the area alone, is also essential for studies concerning planetary-scale processes such as mantle dynamics, plume generation and evolution, and the drivers of the supercontinent cycle. Constituting a volume perturbation with a negative buoyancy force, the time-dependent flux of subducted slabs may contribute to mantle return flow in the form of plume pulses or transient superswells. Superswells are large-scale upwellings of hot mantle material that are believed to contribute to the formation of dynamic elevated topography and associated volcanism when they interact with the lithosphere (McNutt, 1998, Mcnutt and Fischer, 1987). The occurrence of paleo-superswells has been inferred from features such as flat-topped guyots in the Pacific (Darwin Rise) (Menard, 1964), and periods of accelerated continental erosion and denudation (i.e. South African Plateau during the mid- to late-Cretaceous) (Stanley et al., 2015, Menard, 1964).

Using the plate motion model from Müller et al. (2016), we reconstruct subduction zone kinematics since the Late Triassic and compute a number of subduction related parameters to produce a continuous

model of subducting plate area and slab flux. This topological plate motion model is able to capture the dynamic evolution of Earth's tectonic plates in a systematic way that reconciles both the rules of plate tectonics and evidence captured in the geology related to tectonic processes (Gurnis et al., 2012). With the departure from relying simply on the present-day distribution of seafloor ages or a handful of 'snapshots' of plates through time, the model by Müller et al. (2016) allows for the construction of a detailed and direct estimate of subduction evolution for the past 230 Ma.

1.1 History of subduction

Initial attempts at understanding subduction history relied on our knowledge of seafloor production at mid-ocean ridge (MOR) spreading centres, and the link between production and consumption of oceanic lithosphere in the plate motion model. Based on the premise that for all oceanic crust produced, the equivalent area must be consumed at subduction zones to preserve seafloor area, a global seafloor production rate curve can be used as a proxy for the global rate of subduction, giving us an idea of the area of lithosphere consumed per unit time (Rowley, 2002). This preface assumes that on a global scale, plate deformation is negligible. In a more direct approach to constraining the history of subduction, Scrivner and Anderson (1992) used a simple, binary slab distribution function to determine regions of subduction since the break-up of Pangea, estimating subduction locations but not the amount of material that has been consumed. Engebretson et al. (1992) estimated the evolution of subduction based on relative plate motions in a fixed hot spot reference frame (Figure 1). Using stage poles to define plate geometries and interactions, and by assuming that the subduction zones remained fixed relative to the overriding plates, identified subduction zones were reconstructed to their former positions and the total area of subducted lithosphere calculated in 5 Myr intervals. An area of 525 million km^2 of oceanic crust was estimated to have been consumed since 180 Ma, an area close to the surface area of the Earth (Engebretson et al., 1992). This work highlighted differences in convergent margins; one style involving the draping of slabs over a large distributed area, such as under the North American continent, another resulting in a narrow band of layered slabs. This research supported previous results attributing mantle heterogeneities observed from seismic velocities, variations in the geoid and the global distribution of hotspots, to the long-term patterns of global subduction (Richards et al., 1988, Engebretson et al., 1992, Chase, 1979).

Hounslow et al. (2018) present a plate-model based estimate of subducting area through time using the plate motion model from Matthews et al. (2016). 'Subduction area flux (SAF)' was calculated for the period between 410 Ma and present day, with subsequent results used to examine the link between subduction at the surface and geomagnetic polarity reversal rates. In addition to this computed curve, Hounslow et al. (2018) examine the subducting area curve calculated by Vérard et al. (2015) based on proprietary plate reconstructions (0 – 600 Ma), that are not topological. The two plate models from which these curves are derived therefore extend back into the Paleozoic, with Matthews et al. (2016) being the only open access model. To assess the validity of these curves, Hounslow et al. (2018) used two independent subduction flux proxies, a detrital zircon proxy and a mantle strontium isotope proxy from van der Meer et al. (2017). Both proxies aligned best with the Matthews et al. (2016) curve suggesting that this was the more reliable of the two plate reconstructions.

While many studies have investigated the correlation between subduction locations and seismic images of the upper and lower mantle to explore the link between surface and interior processes, a study from Van der Meer et al. (2014) used these images to infer slab flux. The length of subducted slabs was estimated from seismic tomography and used to reconstruct the area of subducted lithosphere since the Triassic by applying a constant rate of subduction and correcting for slab length changes as a result of density reductions and phase changes in the mantle (Figure 1). The lack of temporal resolution, the inconsistencies between tomographic models (of which only one model is used by Van der Meer et al. (2014)), and our limited knowledge of exactly how slabs behave and transform as they move through the mantle, implies that this method is in need of refinement. Without integrating time- and space-dependent convergence rates on at least a regional basis, the method used by Van der Meer et al. (2014) is only suitable for estimating "snapshots" of global subduction zone lengths.

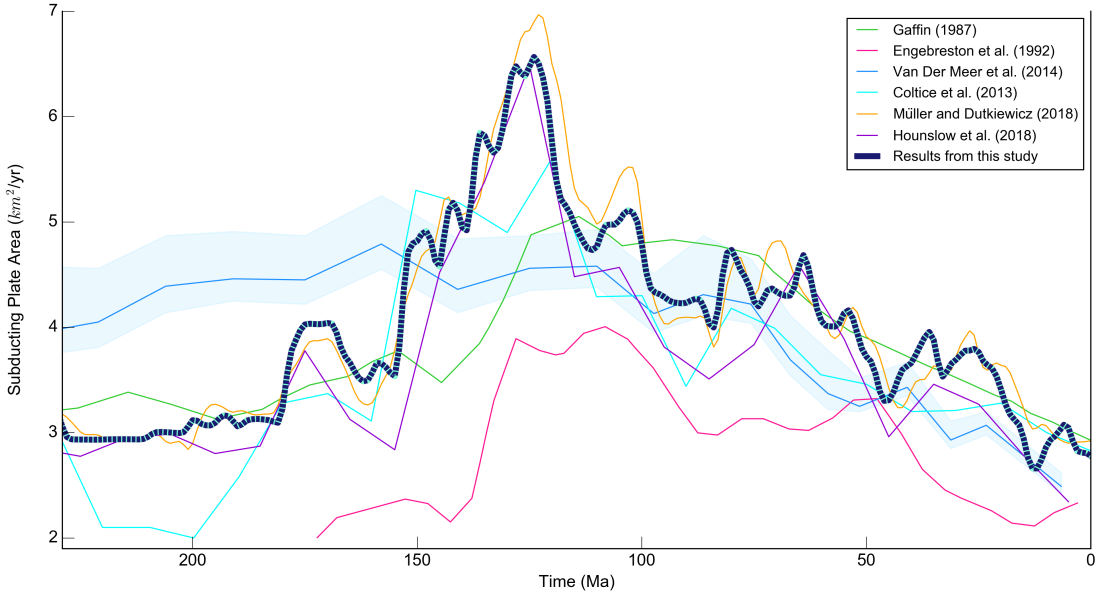

Figure 1. Global subducting seafloor area since the Late Triassic. Time series consist of both direct methods of measurement, as well as proxies, namely, rates of seafloor area production. Green line shows the seafloor production rate curve presented by Gaffin (1987), based on the inversion of long-term sea level change. Bright blue line shows a more recent seafloor production rate curve derived from the plate tectonic reconstructions of Seton et al. (2012) derived by Coltice et al. (2013). The pink line depicts the area of seafloor subducted annually according to relative plate motions within a fixed-hotspot reference frame (Engebretson et al., 1992). Blue line shows the calculated subducting plate area curve based on seismic tomography imaging of subducted slabs (Van der Meer et al., 2014). Purple line depicts the published 'subduction area flux' curve from Hounslow et al. (2018), based on the plate model of Matthews et al. (2016). Orange line depicts the rate of seafloor production through time, based on the plate model used in this study (Müller et al., 2016), constructed using results from Müller and Dutkiewicz (2018). The thick dark blue line presents the results of this study; subducting plate area derived from the plate reconstruction model of Müller et al. (2016). Both the orange and dark blue time series have been filtered using a Gaussian distribution with a standard deviation (σ) of 1.

Estimates of subduction zone length and subducting plate area alone do not provide a complete history of subduction, and hence a volumetric analysis is required, as noted by Wen and Anderson (1995). Using finite plate rotations and seafloor magnetic anomalies to construct present day isochrons, Wen and Anderson (1995) reconstructed the history of subducted seafloor area and slab volume flux for the last 140 Ma. Using a global, dynamic plate model with much refined plate rotations and computed digital age grids of the seafloor, we present an improved and continuous estimate of slab flux for the past 230 Ma. A detailed understanding of this process is useful to elucidate global changes in the plate tectonic cycle, how surface processes are coupled to mantle dynamics, and how carbon and other volatiles are cycled through deep time at a planetary scale.

2 Methodology

In this paper we define *slab flux* as the total volume of oceanic lithosphere consumed globally at subduction zones per unit time, presented in this paper in cubic kilometres per year (km^3yr^{-1}). We define *subducting plate area* as the total area of seafloor subducted globally per unit time, presented in square kilometres per year (km^2yr^{-1}). Although the term *subduction flux* was proposed by Silver and Behn (2008) to define the area of lithosphere being consumed globally, we use the term *subducting plate area* is used to avoid confusion with *slab flux*.

The subduction-related parameters presented in this paper are constructed using the plate reconstruction model from Müller et al. (2016) in conjunction with the open source *GPlates* software (www.gplates.org) and pyGPlates (the Python interface to GPlates). Featuring continuously closing plate polygons, this global plate model provides a continuous description of plate motions since the Late Triassic, along with the ability to compute plate velocity fields globally (Müller et al., 2016). These features allow for the extraction of subduction zone kinematics across the entire surface of the globe at 1 Myr intervals since 230 Ma, and subsequently, calculations of subducting plate area and slab flux. We highlight that prior to 50 Ma the model may be missing subduction zones, and that our results are therefore minimum estimates. We also note that the Müller et al. (2016) plate model used here includes an updated evolution of the Western Tethys (north of Arabia) based on Zahirovic et al. (2016), and with a correction to the Pacific according to Torsvik et al. (2019).

At each time step, the subduction zones are divided into segments with a maximum threshold length of 0.5°, to increase sampling accuracy. The sampling uses the kinematics of the model to extract convergence rates and obliquities, arc lengths, plate IDs and the age of the subducting seafloor (Figure 2). Seafloor ages are taken from paleo-age grids (0.1° grid resolution), which are created using seafloor spreading isochrons at 1 Myr intervals (Müller et al., 2016). For periods and regions where seafloor spreading isochrones are not preserved, the sea floor paleo-age grids are created using simplified synthetic isochrons, constrained by terrane rifting and drifting from paleomagnetic data. For the Pacific, a long-lived triple junction is assumed, which is an oversimplification, but no other approaches are currently workable or reliable. Any anomalous, negative convergence rates are converted to a rate of

zero. We calculate subducting plate area, the area of oceanic lithosphere subducted globally per unit time, as the product of segment length and orthogonal convergence rate, summed for all subduction zone segments.

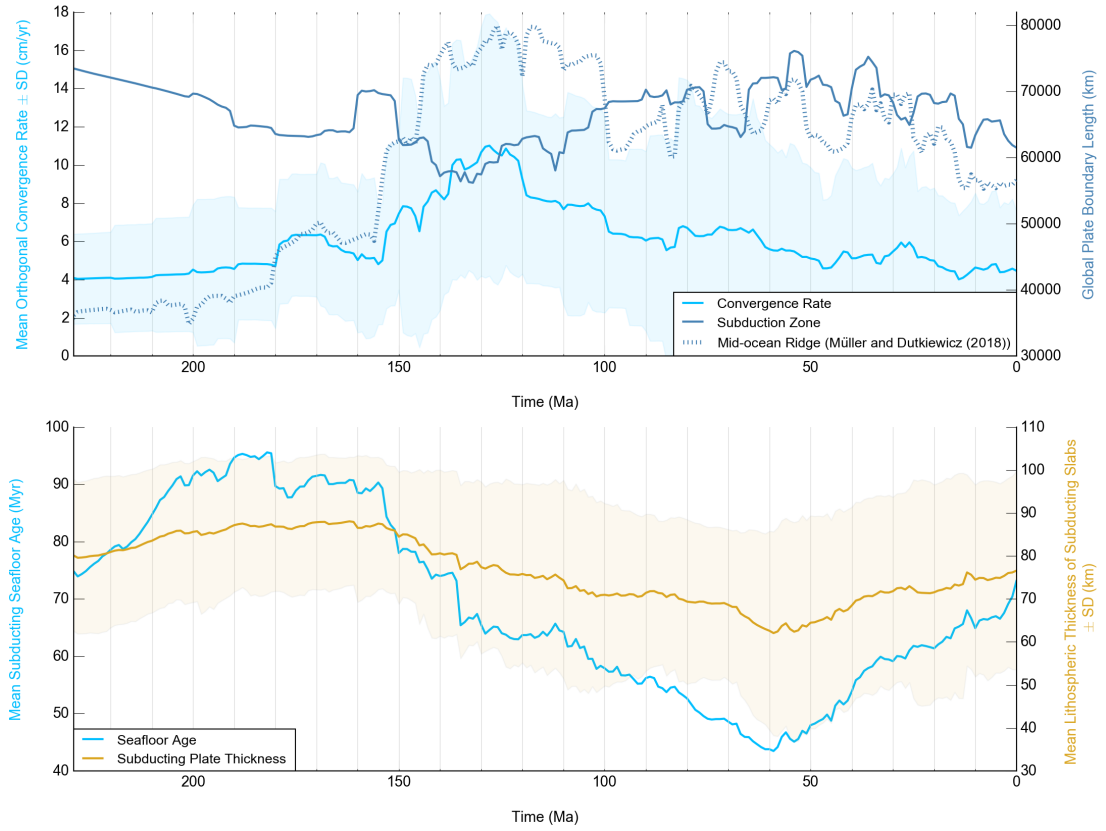

Figure 2. Global subduction parameters since the Late Triassic extracted from the plate model by Müller et al. (2016), using pyGPlates. These parameters are used to calculate slab flux and subducting plate area. Lithospheric thickness was calculated as a function of seafloor age using the plate model of lithospheric cooling developed by Parsons and Sclater (1977). Data has been filtered using a Gaussian distribution with a standard deviation (σ) of 0.5.

Calculating slab flux, the volume of lithosphere consumed globally per unit time, requires knowledge of the subducting plate thickness along each segment, which varies with the age of the seafloor (Crosby et al., 2006, Carlson and Johnson, 1994). A range of numerical models describing plate formation and cooling have been developed (Parsons and Sclater, 1977, Fowler, 2005, Stein and Stein, 1992, Parsons and McKenzie, 1978, Grose, 2012). In this paper we use a plate model of lithospheric cooling with a plate thickness of 125 km following Grose (2012) with the bottom boundary mantle temperature (i.e. temperature at the base of the lithosphere) (T_m) set to 1350°C (Parsons and Sclater, 1977, Grose, 2012). Using the results of this model, slab flux is calculated as the product of segment length, lithospheric thickness and orthogonal convergence rate, summed for all subduction zone segments. The data were subsequently smoothed using a Gaussian filter with a standard deviation (σ) of 1.

It is important to note that the Matthews et al. (2016) model, used by Hounslow et al. (2018) to construct their SAF curve, was created by combining the 0 - 230 Ma Müller et al. (2016) model and the 250 – 410 Ma Domeier and Torsvik (2014) model. We therefore expect a high degree of similarity between our result and that from Hounslow et al. (2018). It should be noted that slight changes in plate kinematics around the period from ~ 200 – 250 Ma arose as a result of stitching these two models together (Matthews et al. (2016).

The potential link between slab flux and the emplacement of large igneous provinces (LIPs) is investigated using two published LIP databases. The first, a database of LIPs compiled and digitized by Johansson et al. (2018) is based primarily on the work of Coffin et al. (2006), Bryan and Ernst (2008) and Ernst (2014). The second database from Whittaker et al. (2015) contains only specifically plume-related LIP products. The eruption duration of all LIPs is set to 3 Myr, following Johansson et al. (2018), to compute the area of actively erupting LIPs since 230 Ma.

3 Results and Discussion

3.1 Subduction history since the Late Triassic

The plate motion model from Müller et al. (2016) implies that global subduction kinematics have varied significantly since the Late Triassic. Both the total area of subducting seafloor and subducting slab volume (slab flux) peaked in the Early Cretaceous at ~ 130 Ma due to fast global average convergence rates following the break up of Pangea (Figure 1, Figure 3). The slab flux peak reached a rate of 530 km^3/yr at 128 Ma, while the maximum rate of subducting seafloor area was 6.8 km^2/yr at 124 Ma. These peaks were followed by an overall decline until present day for both slab flux and subducting plate area with local peaks occurring during the Late Cretaceous (80 Ma) and the Paleogene (50 – 20 Ma). A discussion of the dominant Early Cretaceous slab flux peak is explored in section 3.1.3. Since the Late Triassic (230 Ma), a total of ~ 921 million km^2 of seafloor have been subducted, more than one and a half times the surface area of the Earth. This equates to ~ 70 billion km^3 of slab material being consumed at convergent zones and subducted into the Earth's mantle.

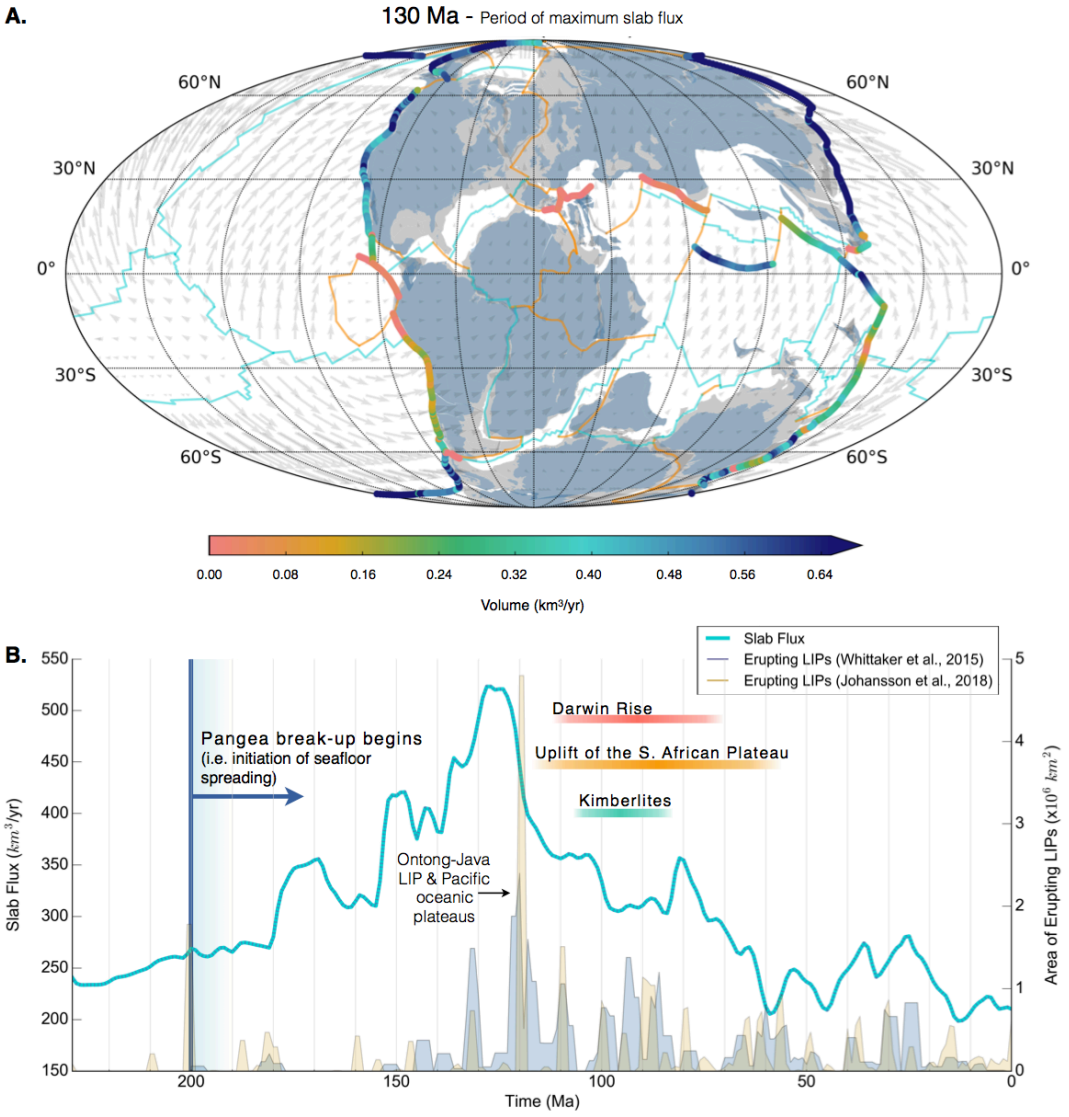

Figure 3. A) Global slab volume flux at 130 Ma, representing the slab flux maximum, based on the plate motion model from Müller et al. (2016). Light and dark grey patterns indicate non-oceanic crust and present-day continents respectively. Grey arrows indicate absolute plate motion velocities. B) Slab flux (light blue curve) constructed using the plate reconstruction model from Müller et al. (2016), with the area of actively erupting LIPs (both continental and oceanic). Yellow signal represents data from Johansson et al. (2018), and the dark blue signal, data from Whittaker et al. (2015), which includes only plume-related products. Eruptions are set to last for 3 Myrs, following Johansson et al. (2018). Areas of erupting LIPs are based off present-day surface expressions, and therefore represent minimum estimates, with uncertainty increasing with the age of the LIP (Johansson et al., 2018). The slab flux curve has been filtered using a Gaussian distribution with a standard deviation (σ) of 1. Dark blue line and arrow indicates the beginning of seafloor spreading during the break-up of Pangea (Müller et al., 2019). The red bar indicates the time period during which the Darwin Rise superswell was likely active and there was elevation of the seafloor (Menard, 1964, McNutt et al., 1990), the orange bar represents the period of uplift and accelerated erosion across the South African Plateau (Said et al., 2015, Stanley et al., 2015), and the green bar indicates the age range of kimberlite intrusions (Jelsma et al., 2004).

273 The total length of subduction zones globally, within the kinematic reconstruction, ranged from a low of
274 ~ 56,000 km during the Early Cretaceous (135 Ma), to a high of ~77,000 km at 55 Ma, with variation
275 lower than overall changes in MOR lengths (Müller and Dutkiewicz, 2018) (Figure 2). The decrease in
276 global subduction zone length during the Late Jurassic was mainly driven by the closure of the Eurasian
277 Mongol-Okhotsk and Arctic South Anuyi ocean basins around 150 and 140 Ma (Shephard et al., 2013,
278 Van der Voo et al., 1999) (Figure 4). Initiation of a number of subduction zones around Southeast Asia
279 during the Cenozoic contributes to the increase in subduction zone lengths during this time (Zahirovic
280 et al., 2014). Orthogonal convergence rates display a reverse trend to subduction zone lengths, peaking
281 during the Early Cretaceous to a mean rate of ~ 11 cm/yr, above an average range of ~ 4 – 7 cm/yr for
282 the past 230 Myr (Figure 2). Fast plate velocities for the Izanagi, Kula and Farallon plates in the north
283 Pacific around 80 Ma led to high convergence rates for subduction zones along the margin of north
284 America and east Asia, resulting in slab flux and subducting plate area peaks at this time (Figure 4, 5).
285 The mean seafloor age of plates being subducted globally increased during the Triassic and remained
286 high into the Jurassic, before sharply decreasing in age until reaching a minimum mean age of ~ 45 Myr
287 during the Paleocene (Figure 2). Mean lithospheric thickness of subducting slabs, roughly co-varying
288 with seafloor age due to the exponential relationship, ranged between ~ 60 and 90 km (Figure 2).
289

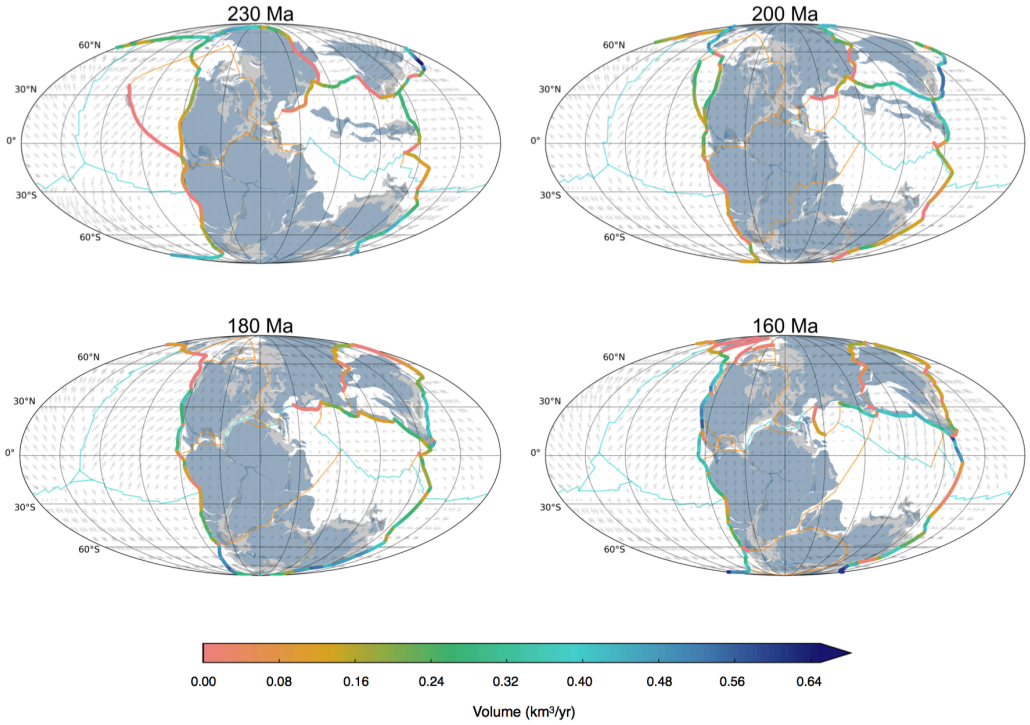

290

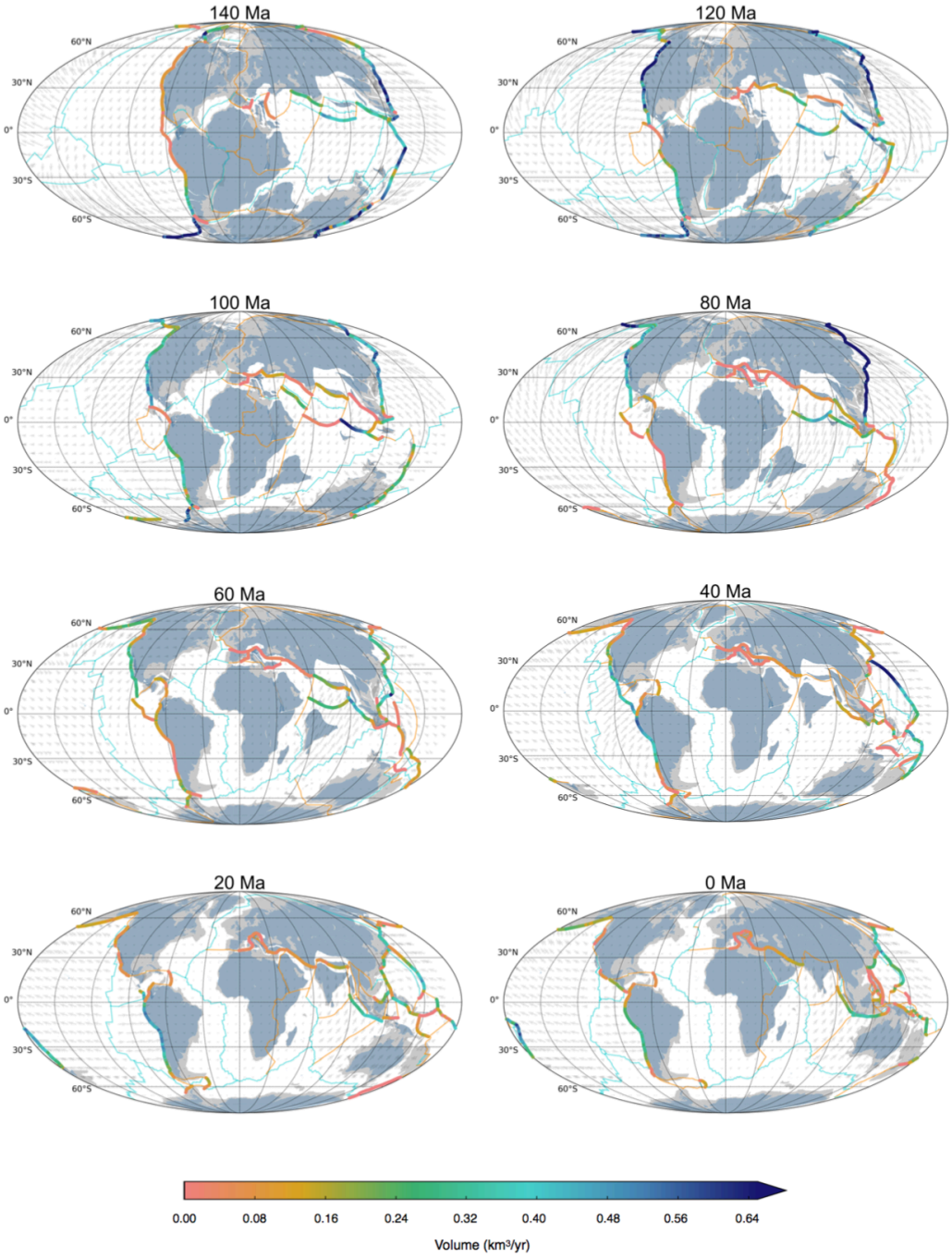

Figure 4. Global slab flux since the Late Triassic using the Müller et al. (2016) plate model. Light and dark grey patterns indicate non-oceanic crust and present-day continents, respectively. Grey arrows indicate absolute plate motion velocities.

3.1.1 Evolution of subducting seafloor area

Figure 1 presents subducting plate area (thick dark line) derived from the Müller et al. (2016) plate motion model, as well as previous estimates and proxies for subducting seafloor area. This comparison reveals that for the last ~ 100 million years, estimates are in fairly good agreement, with an overall decreasing trend from a rate of ~ 4.5 to 3 km^2/yr of subducting seafloor. For times before 100 Ma, the curves diverge, reflecting the growing uncertainties that come with reconstructing plate motions through deeper geological time. Perhaps the greatest deviation from prior estimates is during the period from 150 to 100 Ma, where we see a peak in subducting plate area to higher rates than all previous estimates have predicted, with a maximum rate of 6.8 km^2/yr. While all previous independent curves have estimated a peak in subducting plate area some time in the Cretaceous, they range from between ~ 4 and 5.5 km^2/yr. Interestingly, during the Late Triassic and Jurassic, the closest independent estimates are between our curve and the earliest proxy from Gaffin (1987), constructed using a method of sea level inversion, based on the first-order eustatic sea level curve from Vail et al. (1977).

Given that both our results and those of Hounslow et al. (2018) were constructed from a similar plate motion model for the period spanning 0 – 230 Ma (Müller et al., 2016), we expected to see a high degree of similarity between the two time series – yet they display some noticeable differences, namely in the resolution, their absolute values and slight differences in tends. The Hounslow et al. (2018) curve is presented in 10 Myr intervals (compared to 1 Myr intervals for our curve), a conservative resolution derived from the paleomagnetic data used to inform the plate motions during the Paleozoic period in the Matthews et al. (2016) model. Methods of construction also differed slightly for the two curves (see supplementary material from Hounslow et al. (2018) for their detailed methodology). Essentially, while both methods restricted calculations to plate boundaries specifically labelled as subduction zones in the model, different degrees of filtering were applied, and this along with resolution, influenced the absolute value and trends of the curves.

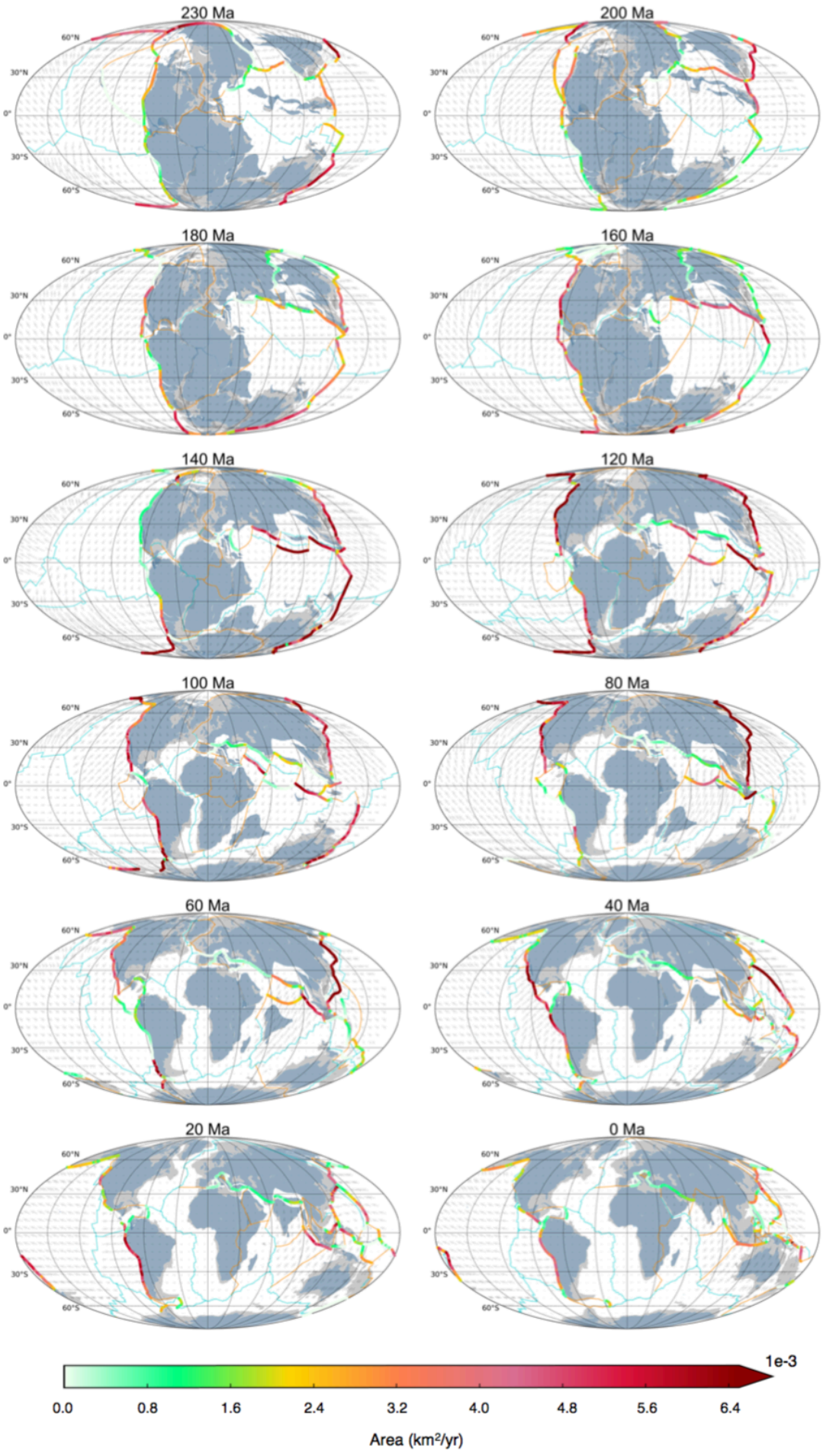
230 Ma
200 Ma
180 Ma
160 Ma
140 Ma
120 Ma
100 Ma
80 Ma
60 Ma
40 Ma
20 Ma
0 Ma
60°N
30°N
0°
30°S
60°S
1e-3
0.0
0.8
1.6
2.4
3.2
4.0
4.8
5.6
6.4
Area (km²/yr)

327

Figure 5. Global subducting plate area since the Late Triassic constructed using the Müller et al. (2016) plate motion model. Light and dark grey patterns indicate non-oceanic crust and present-day continents, respectively. Grey arrows indicate absolute plate motion velocities.

Our results allow us to demonstrate the inaccuracy of using subduction zone length as a proxy for subducting plate area or slab flux, given marked variations in global convergence rates and directions through time. Figure 6 presents a plot of total subduction zone length against the subducting plate area. A correlation coefficient (R) of -0.5, indicates that these time series show differing trends. This result suggests that the method inferring a correspondence between subduction zone length and slab flux adopted by van der Meer et al. (2014), using seismic tomographic interpretations of subducted slabs to estimate subduction zone lengths through time, cannot be used to accurately estimate subduction area or slab flux.

Estimates of subducting seafloor area from plate motion models can be validated against independent subduction flux proxies that capture local changes along actively converging margins or changes in the volume of seafloor being produced, such as isotope or mineral signatures. An independent detrital zircon proxy was constructed by Hounslow et al. (2018) for this specific purpose. Forming in association with magmatic arcs, the age-frequency distribution of zircons holds the potential to track fluctuations in subduction related arc magmatism, and is both a global as well as fairly unbiased temporal estimate. Another useful proxy is given by the mantle derived component of the strontium isotope (van der Meer et al. (2017), which plays a role in modulating the $^{87}Sr/^{86}Sr$ ratio of seawater. Given that the flux of strontium from the mantle is partially governed by the rate of seafloor spreading (itself a valid proxy of subduction flux), we can use this ratio to validate model-based estimates of subducting plate area.

As illustrated by Hounslow et al. (2018), both these proxies support their Matthews et al. (2016) derived curve as a valid and representative plate-model based estimate. Cross-correlation analysis revealed good alignment with the detrital zircon proxy, following a delay of ~ 15 Myr, as well a strong positive correlation with the Sr isotope proxy, with no time delay (Hounslow et al., 2018). The time lag with the zircon proxy was interpreted as the 'crystallization delay' time, representing the lag between slabs entering the mantle and zircons forming within the arc magmas. Given the similarity between our results

to those derived by Hounslow et al. (2018), the proxy validation used by Hounslow et al. (2018) can equally be applied to our results.

3.1.2 Slab flux

The slab volume flux presents similar trends and peaks as is seen for the rate of subducting plate area (Figure 3). This similarity is illustrated in Figure 6 (right) where a close to linear relationship is observed between the two time-series. Points deviating from the 1-to-1 relationship represent time periods when these rates differed, due to the subduction of very old or very young crust. The global mean lithospheric thickness of subducting slabs has not varied dramatically through time, averaging between 70 and 90 km thick (Figure 2), however larger variation may have occurred regionally. The greatest deviation between global slab flux and subducting plate area occurred during the Cretaceous and Early Cenozoic, when mean thickness dropped below 70 km. Regionally, subducting plate area has differed most noticeably from slab flux during periods when very old, thick oceanic crust passed through the subduction zone. Historically this occurred in the Northern Tethys Ocean around 200 Ma, the Mongol-Okhotsk Ocean (~ 180 Ma) and the South Anuyi Ocean (~ 160 Ma). At present day this is occurring in the Eastern Pacific.

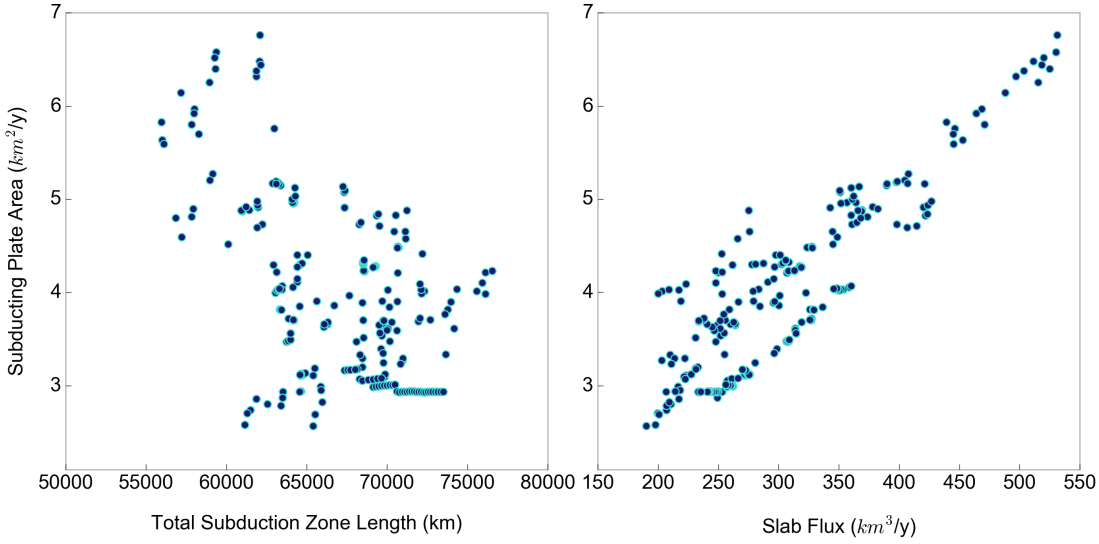

Figure 6. Comparison of subduction zone length, subducting plate area and slab flux for the last 230 Ma. A 1-to-1 linear relationship would indicate that the time series are identical. The relationship between total subduction zone length and subducting plate area is described by a correlation coefficient (R) of – 0.5, while the correlation between slab flux and subducting plate area is given by R = 0.9.

Wen and Anderson (1995) concluded that the region of greatest slab accumulation between 0 - 130 Ma was beneath Southeast Eurasia. Although our results also indicate a large accumulation of material in this region during that period, the main peak in slab volume accumulation occurs beneath the northwestern margin of the Pacific, both for that period and the entire 230 Myr period that our results represent. This change reflects our more detailed, and arguably more robust plate reconstruction. Improved understanding of the extent and timing of subduction along the East Gondwana margin may be one factor contributing to the maximum accumulation we see beneath the northwestern Pacific. This result is illustrated in Figure 7, a map of accumulated slab volume since the Late Triassic. This map also indicates differing styles of subduction. Under the North American continent, slabs have been draped across a broad area, while in the Western Pacific, subduction zones have undergone less migration resulting in a more narrow band of accumulated slabs. These variations in subduction style were noted by Engebretson et al. (1992) and may have implications for mantle convection and the thermal structure of the mantle. The particular style may also influence the way that downgoing slabs interact with and move through the 660 km transition zone (Butterworth et al., 2014). Multiple zones of elevated subducted volume in the Southeast Asia – India region indicate a number of transient subduction events in the plate reconstruction. The broad region of subduction beneath North America displays two regions of particularly large subducted volumes. Sigloch et al. (2008) noticed two distinct stages of subduction beneath North America from multiple-frequency tomography, and that the separation of these occurred between 55 – 40 Ma, as trench migration slowed and the style of subduction changes from flat to steep.

The high slab volume recorded along western Antarctica (Marie Byrd Land) is primarily a result of high plate velocities for the Phoenix/Catequil Plate between ~ 130 and 100 Ma, leading to high convergence rates for the subduction zone along the present Bellingshausen Sea margin (Hochmuth and Gohl, 2017). In the plate motion model used here, a number of the plates that constitute what is now the Pacific Ocean, display high absolute plate velocities during the Mesozoic, reaching speeds above 13 cm/yr and a maximum of 20 cm/yr for the Izanagi. To constrain circum-Pacific convergence velocities during the Mesozoic, large portions of the now subducted Izanagi, Farallon and Phoenix plates need to be reconstructed. A formal assessment of the uncertainties involved in reconstructing now subducted portions of the Panthalassic ocean basin is impossible. However, magnetic lineations in the Pacific

411 Ocean provide robust evidence for a now largely subducted Cretaceous mid-ocean ridge system in the
412 Pacific Ocean, significantly longer than today's ridge system in the Pacific Ocean, implying that the mid-
413 ocean ridge system bounding the Pacific Plate and its adjacent plates can be reconstructed all the way
414 back to the Jurassic (Nakanishi et al., 1992). In the model used here the Izanagi-Farallon-Phoenix triple
415 junction was reconstructed based on these preserved magnetic lineations and the assumption that this
416 triple junction, at which the Pacific Plate warn born around 170 Ma, existed in a similar form since the
417 Triassic (i.e. 230 Ma) – see (Müller et al., 2016) for a detailed discussion on uncertainties involved in these
418 reconstructions.
419
420 *3.1.3 Cretaceous slab superflux*
421
422 Slab flux almost doubled between 180 and 130 Ma (Figure 3), largely driven by circum-Pacific
423 subduction (Figure 4). During this time, the model shows no major increase in global subduction zone
424 lengths, and the mean age of subducting seafloor, and hence the thickness of subducting slabs, shows
425 an overall decline leading up to 130 Ma. Instead, the increased slab flux results from a significant rise in
426 convergence rates from ~ 5 cm/yr in the Jurassic to ~ 11 cm/yr at 130 Ma in the Early Cretaceous. The
427 higher circum-Pacific convergence rates are complemented by the contemporaneous doubling of mid-
428 ocean ridge lengths following the break-up of Pangea from the end Triassic and into the Early
429 Cretaceous (Figure 2, dark blue dashed curve). This increase was a result of the rifting driving the
430 fragmentation of the Pangea supercontinent as well as the initiation of new MORs in Panthalassa
431 (Nakanishi et al., 1992). With a need to preserve planetary surface area, the increase in convergence
432 rates can be traced to the doubling of MOR lengths, suggesting that this was the ultimate driver of the
433 apparent peak in slab flux around 130 Ma. The global average seafloor spreading rate was showing an
434 overall decrease up until 140 Ma, with a small peak occurring between 140 and 120 Ma. Increased
435 seafloor spreading rates was therefore not the significant driver (Müller and Dutkiewicz, 2018).
436
437 The subsequent decline in slab flux from 130 Ma to the present was driven by a combination of slowing
438 convergence rates and subduction of younger, thinner slabs. The decrease in convergence rates may be
439 a result of increasing subduction zone lengths and slightly decreasing MOR lengths. Around 50 Ma,
440 major changes in absolute and relative plate motions resulted in a decrease in global absolute plate

velocities (Müller et al., 2016, Whittaker et al., 2007). This has been in part attributed to an increase in collisional forces and forces resisting plate motion, for example the India and Eurasia collision and subduction of the Izanagi-Pacific Ridge (Rona and Richardson, 1978, Müller et al., 2016).

3.2 Mantle activity in the mid-Cretaceous: a response to slab superflux?

The mid-Cretaceous was characterised by a number of significant geological and climatic perturbations. From ~120 – 80 Ma, a number of oceanic plateaus and large igneous provinces (LIPs) were emplaced during what has been suggested as a 'superplume' episode, dominated by the voluminous eruptions forming the Ontong-Java-Manihiki-Hikurangi plateaus in the Pacific, the Kerguelen plateau in the Indian Ocean and the Paraná-Etendeka province, among many others (Figure 3, 7) (Larson, 1991a, Ernst, 2014, Coffin et al., 2006, Ernst and Youbi, 2017, Madrigal et al., 2016). These eruptions coincide with a prolonged normal magnetic polarity, the Cretaceous Normal Superchron (CNS) (120.6 – 83 Ma), during which the polarity of the Earth's magnetic field was largely stable (Larson, 1991b, Gee and Kent, 2007, Hounslow et al., 2018). A large region in the south-western Pacific, known as the Darwin Rise, also contains evidence of a once active mantle superswell that uplifted the seafloor and fuelled volcanism sometime during the mid-Cretaceous (Menard, 1964, McNutt, 1998). Volcanic kimberlite ages and sedimentation records also suggest superswell driven dynamic uplift beneath the South African Plateau around this time. The mid- to Late Cretaceous was also characterised by a eustatic sea level high, resulting in expansive epicontinental seas, and was dominated by a global greenhouse episode (Hay and Floegel, 2012). We propose that the period of increased slab flux suggested by our results, peaking around 130 Ma in the Early Cretaceous, was a contributing factor and possible trigger of both the major LIP eruptions and active superswells. An increase in the rate of plate material entering the lower mantle, consistently over a period of time or as a series of slab avalanches, may have caused increased vigour of large-scale mantle return flow and influenced the localisation and triggering of plume ascent from the edges of the LLSVPs at the core-mantle boundary (Hassan et al., 2015).

3.2.1 The Cretaceous plume pulse & existing theories

Possible links between major mid-Cretaceous events have been explored since the 1970's. Larson and Pitman (1975) originally proposed the idea that a pulse in seafloor spreading drove the Cretaceous sea level high-stand after the discovery of an extensive MOR system in the Pacific during the Cretaceous. In two influential papers from 1991, building on this conceptual idea, Larson constructed a model linking a number of Cretaceous anomalies to the arrival of one or more large plumes ('superplumes') from the deep mantle (i.e. core-manlte boundary) beneath the Pacific. Larson cites the Ontong-Java and Manihiki Plateaus, among others, as the evidence for one of these major plumes in the Pacific, and suggests that the South Pacific Superswell may be the present day remnant of such a plume (Larson, 1991b, Larson, 1991a). The Ontong-Java-Hikurangi-Manihiki Plateaus are the largest LIPs in the western Pacific. With similar geochemistry and petrology, a number of studies favour a joint emplacement, before subsequent breakup (Taylor, 2006, Hochmuth et al., 2015). Uncertainty still remains as to whether they formed as the result of one or a number of mantle plumes – emplaced material could have been sourced from a single large plume, separate domains within a single plume, a single upwelling splitting before partial melting occurred, or as two compositionally different plumes in spatial proximity (Golowin et al., 2018). In his model, Larson attributed this 'superplume' to the initiation of the Cretaceous Normal Superchron (Larson, 1991b, Larson, 1991a), as well as driving a 50 – 100% increase in oceanic crustal production (MOR and oceanic plateaus combined).

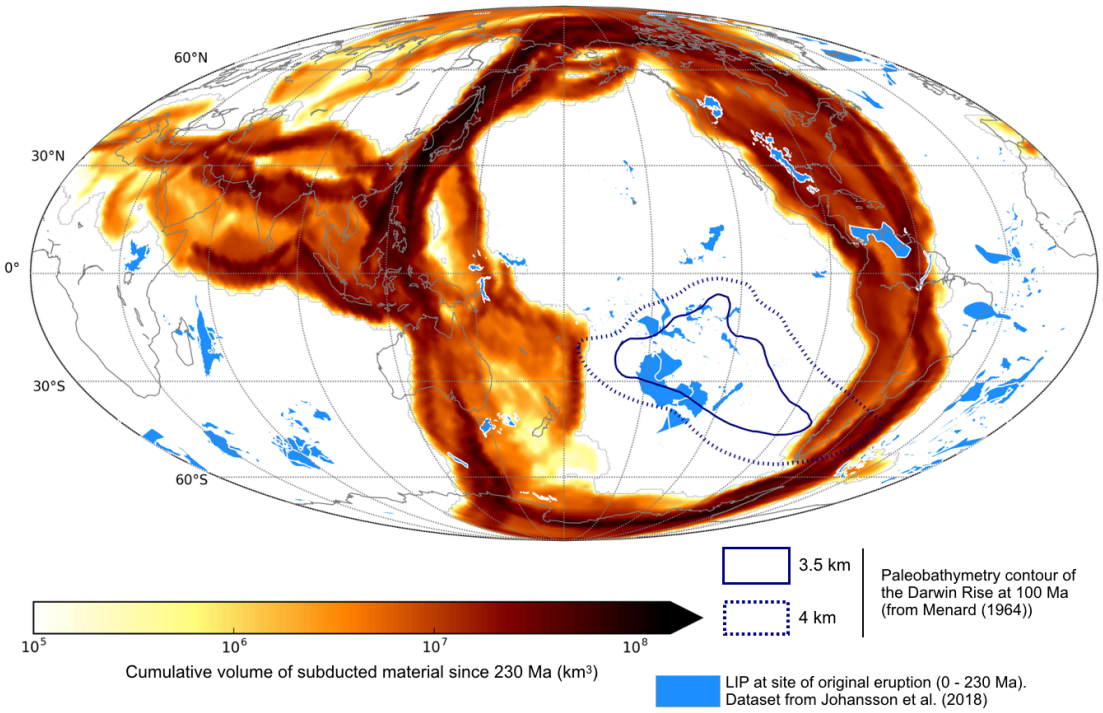

Figure 7. Cumulative slab flux for the past 230 million years with large igneous provinces plotted in blue in the location of their initial eruption. Present day coastlines are outlined in grey, LIP outlines come from Whittaker et al. (2015).

In response to criticism concerning the lag time between deep and surface signals, Larson and Kincaid (1996) later extended the crustal production-superchron model by incorporating a component of sudden slab avalanche/penetration through the 660 km mantle transition zone as the trigger for a superplume event (Larson and Kincaid, 1996, Loper, 1992). This process has been modelled by Tackley et al (1993), where a slab avalanche is triggered following the accumulation of slab material at the transition zone. Recently, Yang et al. (2016) numerically modelled the 'slab avalanche' phenomenon, suggesting that an accumulation of deflected slabs lying sub-horizontally within the transition zone will penetrate suddenly into the lower mantle when the negative buoyancy force surpasses the support of the 660km discontinuity. Increasing in speed as they sink through the lower mantle, these events can trigger a change in mantle flow from layered to whole mantle convection and drive strong downwelling around the sinking slabs (Machetel and Weber, 1991, Peltier and Solheim, 1992, Tackley et al., 1993). This perturbation to the lower mantle, as well as influencing patterns and magnitude of flow, may drive changes in trench motion, continental rifting and topography (Yang et al., 2016). Larson and Kincaid (1996) proposed that such a slab avalanche could cause a rapid upwards advection of the 670 km discontinuity initiating almost immediate near-surface melting, followed eventually by the arrival of

plumes from the core-mantle boundary. Stein and Hofmann (1994) incorporate episodes of major slab penetration into their model of mantle overturn and convection, suggesting that they trigger a catastrophic change from layered to whole mantle convection and the production of major plumes. Slab avalanche episodes have also been proposed as a key component of the supercontinent cycle initiating a pulse in plume generation and the production of juvenile crust (Condie, 1998). Besides evidence of subducted slabs accumulating at the 660 km discontinuity from seismic tomography (Butterworth et al., 2014), time-dependent evidence in support of these occurrences has been lacking.

Figure 7 presents our subducting slab volume flux, overlain with the signal of LIP eruptions and volcanic provinces since the Late Triassic constructed from the LIP databases of Johansson et al. (2018) and Whittaker et al. (2015). The largest peak in erupting areas for both LIP signals at ~ 120 Ma represents the eruption of the Ontong-Java-Manihiki-Hikurangi super-plateau among others, at the beginning of the Cretaceous 'superplume' event. These eruptions appear to begin ~ 10 Myr after the global peak in slab flux, and following almost 50 Myrs of progressively increasing flux into the mantle. During the period from 180 to 120 Ma, ~ 2.40×10^{10} km^3 of slab material was subducted, representing one third of the total volume that has been subducted since the Late Triassic (230 Ma). Based on the timing of these events and the immense volume of material subducted prior to 120 Ma, our results support the model of Larson and Kincaid (1996), citing that a plausible trigger of the Cretaceous 'superplume' LIP eruptions was an immense volume of slab material penetrating into the lower mantle, possibly as a series of slab avalanches, causing a contemporaneous volume perturbation.

Geological evidence indicates that slab sinking rates in the upper mantle can vary between 30 and 70 mm/yr, faster than lower mantle rates due to the large viscosity contrast across the 660 km phase transition (Butterworth et al., 2014, Schellart and Spakman, 2012). In mantle convection modelling, imposing this range of sinking rates often places material much deeper in the mantle than is interpreted from seismic imaging. The most likely explanation for this is that slabs are often stalled at the transition zone as they descend. Evidence suggests that slabs may stall for between 10 and 20 Myrs or that they may even become stagnant along this boundary indefinitely (Pysklywec and Mitrovica, 1998, Butterworth et al., 2014). Some evidence suggests that regions dominated by subduction are associated with faster slab sinking rates, and that the rate of trench migration will play a role in the passage of the slab

through the transition zone, with higher migration rates favouring draping at the transition zone (Stegman et al., 2010, Christensen, 1996). If we assume an upper mantle slab sinking rate of ~ 50 mm/yr (a rough global average) (Butterworth et al., 2014), then slabs will take ~ 10 -15 Myrs to descend to the transition zone. If we consider the effects of stalling, then it may take a minimum of 20 Myrs before slabs subducted at the surface will finally penetrate into the lower mantle (Butterworth et al., 2014). Below migrating subduction zones this may have been in the form of sudden slab avalanches. In regions with slow migration rates where slabs were deposited on top of one another (e.g. along (north-)east Asia during the slab superflux period ~ 180 – 130 Ma), penetration into the lower mantle may have occurred more quickly and continuously with limited stalling. Considering these transit times through the upper mantle, although slabs subducted during the Cretaceous superflux event may not have reached the CMB in time to nucleate new plumes as part of the LIP pulse, the volume perturbation could have fuelled a pulse of LIP eruption by tapping into existing plumes or may have generated near-surface melting associated with accelerated advection and return flow (i.e. superswell) (Hassan et al., 2015).

3.2.2 Superswells: The Darwin Rise and southern Africa

In addition to the role of slab flux perturbations in the LIP emplacements during the Cretaceous, we also suggest that this peak in downgoing material may have contributed to the generation of superswells, such as the one that produced the Darwin Rise and a period of accelerated uplift and erosion across southern Africa during the mid- to late-Cretacous (Said et al., 2015, Stanley et al., 2015, Moore et al., 2009). The Darwin Rise is a region in the south-west Pacific that was the site of broad regional uplift and volcanism during the Cretaceous. First recognised by Charles Darwin in 1845, the region was named in his honour by H.W. Menard in 1964. The region has not been well defined since its first appraisal by Menard (1964), where he defined it as an area covering ~ 10 000 x 4 000 km from the Taumotu Archipelago to the Marshall Islands (Stein and Stein, 1993). The history of uplift in the region has been pieced together by examining the many guyots and coral atolls in the region that contain evidence of subaerial exposure, including during the Cretaceous sea level high-stand, followed by subsidence (Menard, 1964, Menard, 1984, Hamilton, 1956). Menard (1964) proposed that this regional uplift occurred at ~ 100 Ma, while further analysis by McNutt et al. (1990) suggests broad uplift closer to

113 ± 8 Ma. These age constraints place the event sometime in the mid-Cretaceous, in temporal proximity to the period of major slab flux suggested by our results.

Explanations for the existence of the Darwin Rise have centred around mantle plumes (Morgan, 1972), superplumes (Larson, 1991a), and superswells (Mcnutt and Fischer, 1987). Both the East Pacific Rise and the South Pacific Superswell have been cited as present day analogues for the Darwin Rise (Menard, 1984, Mcnutt and Fischer, 1987). The prevalent explanation is the existence of a superswell, suggested by Mcnutt and Fischer (1987) to represent buoyant mantle upwelling on the scale of several thousands of kilometres that produces an anomalously shallow region of the seafloor, and containing a dense clustering of volcanic hot spot products (McNutt, 1998). It is plausible that the major increase in slab material entering the viscous mantle in the Early to mid-Cretaceous, could have triggered a large-scale return flow of hot buoyant material, generating the superswell that produced the Darwin Rise.

There is also evidence to suggest the existence of a superswell beneath the South African Plateau around the same time. Evidence from sedimentary records and volcanic kimberlite ages points to a major period of dynamic uplift and near surface melting during the mid- to late-Cretaceous (Said et al., 2015, Stanley et al., 2015, Moore et al., 2009). Said et al. (2015) propose a period of accelerated erosion into the southern Mozambique passive margin, beginning in the in the mid- to late-Cretaceous, which may have continued until as recently as ~65 Ma. Overlapping with an episode of kimberlite intrusions (~ 90 – 100 Ma (Jelsma et al., 2004, Jelsma et al., 2009)), Said et al. (2015) support the conclusion that mantle buoyancy forces were the cause of uplift, and the subsequent acceleration in erosion and deposition. A mantle upwelling in the form of a superswell would also explain the origin of the kimberlite intrusions. Stanley et al. (2015) also point to a wave of erosion across the Southern African craton from ~ 120 to < 60 Ma, with a pronounced phase of regional erosion (off-craton) between ~ 110 – 90 Ma, citing a dynamic buoyancy source from the mantle as the likely cause of the heightened elevation during this period. The timing of this dynamic uplift, during the mid- to late-Cretacous, supports the argument that another mantle superswell, similar to the one producing the Darwin Rise, was active beneath Southern Africa following the period of slab superflux. This suggests a global mantle response to the Cretaceous slab superflux, triggering the Cretaceous plume pulse and contemporaneous mantle superswells. We suggest that slab superflux may be a general feature of

601 continental dispersal following supercontinent breakup, during the first ~100 my following breakup,
602 driven by the associated vast increase in mid-ocean ridge length. In this case, both a peak in large
603 igneous province generation as well as the formation of enhanced superswell dynamic topography
604 would be expected following supercontinent breakup.
605
606 *3.3 Future work*
607
608 Digital geological maps may hold the clue to identifying major periods of large-scale continental uplift,
609 reflecting transient superswells, via hiatus surface mapping (Friedrich, 2019). A future synthesis of
610 continental hiatuses with conventional thermochronology data may reveal at what times and locations
611 paleo-superswells have existed, and how they related to supercontinent cycles. The erosional products
612 of continental superswell-driven uplift are deposited in adjacent basins and continental margins,
613 implying that basin stratigraphy and time-dependent sedimentation rates can be integrated into
614 analyses and models of continental uplift (e.g. Said et al. (2015)). An additional focus of future work
615 should be to better constrain plate motions and boundary configurations within Panthalassa and
616 explore the possible range of anomalously high plate velocities in this region during the Jurassic and
617 Cretaceous periods. Adjoint mantle convection models (e.g. Colli et al. (2018)) hold the promise to
618 potentially reveal the possible connection between slab superflux and the time dependence of
619 superswells.
620
621 ## 4 Conclusions
622
623 Enabled by the recent evolution in digital plate motion models with topological plate polygons (Müller
624 et al., 2016, Merdith et al., 2017, Gurnis et al., 2012), this study presents a complete history of
625 subducting plate area and slab flux since the Late Triassic. Our results suggest the following:
626 - The rates of both slab flux and subducting plate area peaked during the Early Cretaceous
627 around 130 – 120 Ma.
628 - During the period from 180 Ma to ~ 130 Ma, coinciding with the break-up of Pangea, both
629 rates close to doubled.

- This ~ 50 Myr period of increasing slab flux and subducting plate area was driven primarily by an increase in MOR lengths, predominantly in the Pacific. This increase, coupled with a gradual decrease in global subduction zone lengths, led to higher convergence rates, and thus the flux of oceanic lithosphere into the mantle.
- Global subduction zone lengths alone do not provide a reasonable proxy of subducting plate area or slab flux due to significant temporal and spatial changes in convergence rates and lithospheric thickness.
- Significant slab flux into the mantle during the Cretaceous may have contributed, even triggered, the voluminous eruptions of the Ontong-Java-Manihiki-Hikurangi and Kerguelen plateaus, among others, around 120 Ma, as well as the superswells responsible for the Darwin Rise and the elevation of the South African Plateau during the mid- to late-Cretaceous.
- Slab superflux, a pulse in Large Igneous Province formation and enhanced superswell dynamic topography may all be features of the ~100 Myr period following supercontinent breakup.

Subduction zones shape both Earth's surface and the dynamics of the mantle below. This first order understanding of how convergence along subduction zones has evolved provides a platform from which more complex processes can be studied. A practical application of these results will involve integration of the subducting plate area model into existing carbon box and geochemical models as a tectonic degassing parameter (e.g. the COPSE model (Bergman et al., 2004) and the GEOCARBSULF model (Berner, 2006)). Arc volcanoes associated with subduction zones, along with MORs and hot spots, play a major role in the exchange of carbon and other volatiles between deep (mantle) and shallow (surface) reservoirs over geological timescales (Bergman et al., 2004). This improved understanding of how subduction flux has changed since the Late Triassic and during the break up of Pangea may lead to greater insights concerning the coupling of deep and surface processes, including triggering of mantle return flow and plumes, as well as possible temporal offsets between these processes, resulting from large perturbations of the slab flux.

5 Acknowledgments

ME, SZ and RDM were supported by Alfred P Sloan grants G-2017-9997 and G-2018-11296 through the Deep Carbon Observatory. SZ, RDM, and SW were supported by Australian Research Council grant IH130200012. RDM was also supported by the AuScope National Collaborative Research Infrastructure System (NCRIS) program.

6 Competing Interests

None.

References

BERGMAN, N. M., LENTON, T. M. & WATSON, A. J. 2004. COPSE: a new model of biogeochemical cycling over Phanerozoic time. American Journal of Science, 304, 397-437.

BERNER, R. A. 1994. GEOCARB II: A revised model of atmospheric CO2 over phanerozoic time American Journal of Science; (United States), 294.

BERNER, R. A. 2006. GEOCARBSULF: a combined model for Phanerozoic atmospheric O 2 and CO 2. Geochimica et Cosmochimica Acta, 70, 5653-5664.

BRYAN, S. E. & ERNST, R. E. 2008. Revised definition of large igneous provinces (LIPs). Earth-Science Reviews, 86, 175-202.

BUTTERWORTH, N., TALSMA, A., MÜLLER, R., SETON, M., BUNGE, H.-P., SCHUBERTH, B., SHEPHARD, G. & HEINE, C. 2014. Geological, tomographic, kinematic and geodynamic constraints on the dynamics of sinking slabs. Journal of Geodynamics, 73, 1-13.

CARLSON, R. L. & JOHNSON, H. P. 1994. On modeling the thermal evolution of the oceanic upper mantle: An assessment of the cooling plate model. Journal of Geophysical Research: Solid Earth, 99, 3201-3214.

CHASE, C. G. 1979. Subduction, the geoid, and lower mantle convection. Nature, 282, 464.

CHRISTENSEN, U. R. 1996. The influence of trench migration on slab penetration into the lower mantle. Earth and Planetary Science Letters, 140, 27-39.

COFFIN, M. F., DUNCAN, R. A., ELDHOLM, O., FITTON, J. G., FREY, F. A., LARSEN, H. C., MAHONEY, J. J., SAUNDERS, A. D., SCHLICH, R. & WALLACE, P. J. 2006. Large igneous provinces and scientific ocean drilling: Status quo and a look ahead. Oceanography, 19, 150-160.

COLLI, L., GHELICHKHAN, S., BUNGE, H.-P. & OESER, J. 2018. Retrodictions of Mid Paleogene mantle flow and dynamic topography in the Atlantic region from compressible high resolution adjoint mantle convection models: Sensitivity to deep mantle viscosity and tomographic input model. Gondwana Research, 53, 252-272.

COLTICE, N., SETON, M., ROLF, T., MÜLLER, R. & TACKLEY, P. J. 2013. Convergence of tectonic reconstructions and mantle convection models for significant fluctuations in seafloor spreading. Earth and Planetary Science Letters, 383, 92-100.

CONDIE, K. C. 1998. Episodic continental growth and supercontinents: a mantle avalanche connection? Earth and Planetary Science Letters, 163, 97-108.

CROSBY, A., MCKENZIE, D. & SCLATER, J. 2006. The relationship between depth, age and gravity in the oceans. Geophysical Journal International, 166, 553-573.

DOMEIER, M. & TORSVIK, T. H. 2014. Plate tectonics in the late Paleozoic. Geoscience Frontiers, 5, 303-350.

ENGEBRETSON, D. C., KELLEY, K. P., CASHMAN, H. & RICHARDS, M. A. 1992. 180 million years of subduction. GSA today, 2, 93-100.

ERNST, R. E. 2014. Large igneous provinces, Cambridge University Press.

ERNST, R. E. & YOUBI, N. 2017. How Large Igneous Provinces affect global climate, sometimes cause mass extinctions, and represent natural markers in the geological record. Palaeogeography, Palaeoclimatology, Palaeoecology, 478, 30-52.

FOWLER, C. M. R. 2005. The Solid Earth: An Introduction to Global Geophysics United Kingdom, Cambridge University Press.

FRIEDRICH, A. M. 2019. Palaeogeological hiatus surface mapping: a tool to visualize vertical motion of the continents. *Geological Magazine*, 1-12.
GAFFIN, S. 1987. Ridge volume dependence on seafloor generation rate and inversion using long term sealevel change. *American Journal of Science,* 287, 596-611.
GEE, J. S. & KENT, D. V. 2007. Source of oceanic magnetic anomalies and the geomagnetic polarity time scale. *Treatise on Geophysics, vol. 5: Geomagnetism*, 455-507.
GOLOWIN, R., PORTNYAGIN, M., HOERNLE, K., HAUFF, F., WERNER, R. & GARBE-SCHÖNBERG, D. 2018. Geochemistry of deep Manihiki Plateau crust: Implications for compositional diversity of large igneous provinces in the Western Pacific and their genetic link. *Chemical Geology*.
GROSE, C. J. 2012. Properties of oceanic lithosphere: Revised plate cooling model predictions. *Earth and Planetary Science Letters,* 333, 250-264.
GURNIS, M., TURNER, M., ZAHIROVIC, S., DICAPRIO, L., SPASOJEVIC, S., MÜLLER, R. D., BOYDEN, J., SETON, M., MANEA, V. C. & BOWER, D. J. 2012. Plate tectonic reconstructions with continuously closing plates. *Computers & Geosciences,* 38, 35-42.
HAMILTON, E. L. 1956. *Sunken islands of the mid-Pacific mountains*, Geological Society of America.
HASSAN, R., FLAMENT, N., GURNIS, M., BOWER, D. J. & MÜLLER, D. 2015. Provenance of plumes in global convection models. *Geochemistry, Geophysics, Geosystems,* 16, 1465-1489.
HAY, W. W. & FLOEGEL, S. 2012. New thoughts about the Cretaceous climate and oceans. *Earth-Science Reviews,* 115, 262-272.
HOCHMUTH, K. & GOHL, K. 2017. Collision of Manihiki Plateau fragments to accretional margins of northern Andes and Antarctic Peninsula. *Tectonics,* 36, 229-240.
HOCHMUTH, K., GOHL, K. & UENZELMANN‐NEBEN, G. 2015. Playing jigsaw with large igneous provinces—A plate tectonic reconstruction of Ontong Java Nui, West Pacific. *Geochemistry, Geophysics, Geosystems,* 16, 3789-3807.
HOFMANN, A. 1997. Mantle geochemistry: the message from oceanic volcanism. *Nature,* 385, 219.
HOUNSLOW, M. W., DOMEIER, M. & BIGGIN, A. J. 2018. Subduction flux modulates the geomagnetic polarity reversal rate. *Tectonophysics*.
JELSMA, H., BARNETT, W., RICHARDS, S. & LISTER, G. 2009. Tectonic setting of kimberlites. *Lithos,* 112, 155-165.
JELSMA, H. A., DE WIT, M. J., THIART, C., DIRKS, P. H., VIOLA, G., BASSON, I. J. & ANCKAR, E. 2004. Preferential distribution along transcontinental corridors of kimberlites and related rocks of Southern Africa. *South African Journal of Geology,* 107, 301-324.
JOHANSSON, L., ZAHIROVIC, S. & MÜLLER, R. D. 2018. The interplay between the eruption and weathering of Large Igneous Provinces and the deep‐time carbon cycle. *Geophysical Research Letters*.
LARSON, R. 1991a. Latest pulse of Earth: Evidence for a mid-Cretaceous superplume. *Geology,* 19, 547-550.
LARSON, R. L. 1991b. Geological consequences of superplumes. *Geology,* 19, 963-966.
LARSON, R. L. & KINCAID, C. 1996. Onset of mid-Cretaceous volcanism by elevation of the 670 km thermal boundary layer. *Geology,* 24, 551-554.
LARSON, R. L. & PITMAN , W. C. 1975. World-Wide Correlation of Mesozoic Magnetic Anomalies and Its Implications: Discussion and Reply: Reply. *Geological Society of America Bulletin,* 86, 270-272.
LOPER, D. E. 1992. On the correlation between mantle plume flux and the frequency of reversals of the geomagnetic field. *Geophysical Research Letters,* 19, 25-28.
MACHETEL, P. & WEBER, P. 1991. Intermittent layered convection in a model mantle with an endothermic phase change at 670 km. *Nature,* 350, 55-57.
MADRIGAL, P., GAZEL, E., FLORES, K. E., BIZIMIS, M. & JICHA, B. 2016. Record of massive upwellings from the Pacific large low shear velocity province. *Nature communications,* 7, 13309.
MATTHEWS, K. J., MALONEY, K. T., ZAHIROVIC, S., WILLIAMS, S. E., SETON, M. & MULLER, D. 2016. Global plate boundary evolution and kinematics since the late Paleozoic. *Global and Planetary Change,* 146, 226-250.
MCNUTT, M., WINTERER, E., SAGER, W., NATLAND, J. & ITO, G. 1990. The Darwin Rise: a Cretaceous superswell? *Geophysical Research Letters,* 17, 1101-1104.
MCNUTT, M. K. 1998. Superswells. *Reviews of Geophysics,* 36, 211-244.
MCNUTT, M. K. & FISCHER, K. M. 1987. The south Pacific superswell. *Seamounts, Islands, and Atolls,* 43, 25-34.
MENARD, H. 1984. Darwin reprise. *Journal of Geophysical Research: Solid Earth,* 89, 9960-9968.
MENARD, H. W. 1964. Marine geology of the Pacific.
MERDITH, A. S., COLLINS, A. S., WILLIAMS, S. E., PISAREVSKY, S., FODEN, J. D., ARCHIBALD, D. B., BLADES, M. L., ALESSIO, B. L., ARMISTEAD, S. & PLAVSA, D. 2017. A full-plate global reconstruction of the Neoproterozoic. *Gondwana Research,* 50, 84-134.
MOORE, A., BLENKINSOP, T. & COTTERILL, F. 2009. Southern African topography and erosion history: plumes or plate tectonics? *Terra Nova,* 21, 310-315.
MORGAN, W. J. 1972. Deep mantle convection plumes and plate motions. *AAPG bulletin,* 56, 203-213.
MÜLLER, R. D. & DUTKIEWICZ, A. 2018. Oceanic crustal carbon cycle drives 26-million-year atmospheric carbon dioxide periodicities. *Science Advances,* 4.
MÜLLER, R. D., SETON, M., ZAHIROVIC, S., WILLIAMS, S. E., MATTHEWS, K. J., WRIGHT, N. M., SHEPHARD, G. E., MALONEY, K. T., BARNETT-MOORE, N. & HOSSEINPOUR, M. 2016. Ocean basin evolution and global-scale plate reorganization events since Pangea breakup. *Annual Review of Earth and Planetary Sciences,* 44, 107-138.

MÜLLER, R. D., ZAHIROVIC, S., WILLIAMS, S. E., CANNON, J., SETON, M., BOWER, D. J., TETLEY, M. G., HEINE, C., LE BRETON, E. & LIU, S. 2019. A global plate model including lithospheric deformation along major rifts and orogens since the Triassic. *Tectonics*.

NAKANISHI, M., TAMAKI, K. & KOBAYASHI, K. 1992. A new Mesozoic isochron chart of the northwestern Pacific Ocean: Paleomagnetic and tectonic implications. *Geophysical Research Letters,* 19**,** 693-696.

PARSONS, B. & MCKENZIE, D. 1978. Mantle convection and the thermal structure of the plates. *J. geophys. Res,* 83**,** 4485-4496.

PARSONS, B. & SCLATER, J. G. 1977. An analysis of the variation of ocean floor bathymetry and heat flow with age. *Journal of geophysical research,* 82**,** 803-827.

PELTIER, W. & SOLHEIM, L. 1992. Mantle phase transitions and layered chaotic convection. *Geophysical Research Letters,* 19**,** 321-324.

PYSKLYWEC, R. N. & MITROVICA, J. X. 1998. Mantle flow mechanisms for the large-scale subsidence of continental interiors. *Geology,* 26**,** 687-690.

RICHARDS, M. A., HAGER, B. H. & SLEEP, N. H. 1988. Dynamically supported geoid highs over hotspots: Observation and theory. *Journal of Geophysical Research: Solid Earth,* 93**,** 7690-7708.

RONA, P. A. & RICHARDSON, E. S. 1978. Early Cenozoic global plate reorganization. *Earth and Planetary Science Letters,* 40**,** 1-11.

ROWLEY, D. B. 2002. Rate of plate creation and destruction: 180 Ma to present. *Geological Society of America Bulletin,* 114**,** 927-933.

SAID, A., MODER, C., CLARK, S. & GHORBAL, B. 2015. Cretaceous–Cenozoic sedimentary budgets of the Southern Mozambique Basin: Implications for uplift history of the South African Plateau. *Journal of African Earth Sciences,* 109**,** 1-10.

SCHELLART, W. & SPAKMAN, W. 2012. Mantle constraints on the plate tectonic evolution of the Tonga–Kermadec–Hikurangi subduction zone and the South Fiji Basin region. *Australian Journal of Earth Sciences,* 59**,** 933-952.

SCRIVNER, C. & ANDERSON, D. L. 1992. The effect of post Pangea subduction on global mantle tomography and convection. *Geophysical research letters,* 19**,** 1053-1056.

SETON, M., MÜLLER, R., ZAHIROVIC, S., GAINA, C., TORSVIK, T., SHEPHARD, G., TALSMA, A., GURNIS, M., TURNER, M. & MAUS, S. 2012. Global continental and ocean basin reconstructions since 200Ma. *Earth-Science Reviews,* 113**,** 212-270.

SHEPHARD, G. E., MATTHEWS, K. J., HOSSEINI, K. & DOMEIER, M. 2017. On the consistency of seismically imaged lower mantle slabs. *Scientific Reports,* 7**,** 10976.

SHEPHARD, G. E., MÜLLER, R. D. & SETON, M. 2013. The tectonic evolution of the Arctic since Pangea breakup: Integrating constraints from surface geology and geophysics with mantle structure. *Earth-Science Reviews,* 124**,** 148-183.

SIGLOCH, K., MCQUARRIE, N. & NOLET, G. 2008. Two-stage subduction history under North America inferred from multiple-frequency tomography. *Nature Geoscience,* 1**,** 458.

SILVER, P. G. & BEHN, M. D. 2008. Intermittent plate tectonics? *science,* 319**,** 85-88.

STANLEY, J. R., FLOWERS, R. M. & BELL, D. R. 2015. Erosion patterns and mantle sources of topographic change across the southern African Plateau derived from the shallow and deep records of kimberlites. *Geochemistry, Geophysics, Geosystems,* 16**,** 3235-3256.

STEGMAN, D., SCHELLART, W. & FREEMAN, J. 2010. Competing influences of plate width and far-field boundary conditions on trench migration and morphology of subducted slabs in the upper mantle. *Tectonophysics,* 483**,** 46-57.

STEIN, C. A. & STEIN, S. 1992. A model for the global variation in oceanic depth and heat flow with lithospheric age. *Nature,* 359**,** 123-129.

STEIN, C. A. & STEIN, S. 1993. Constraints on Pacific midplate swells from global depth‐age and heat flow‐age models. *The Mesozoic Pacific: geology, tectonics, and volcanism***,** 53-76.

STEIN, M. & HOFMANN, A. 1994. Mantle plumes and episodic crustal growth. *Nature,* 372**,** 63.

TACKLEY, P. J., STEVENSON, D. J., GLATZMAIER, G. A. & SCHUBERT, G. 1993. Effects of an endothermic phase transition at 670 km depth in a spherical model of convection in the Earth's mantle. *Nature,* 361**,** 699.

TAYLOR, B. 2006. The single largest oceanic plateau: Ontong Java–Manihiki–Hikurangi. *Earth and Planetary Science Letters,* 241**,** 372-380.

TORSVIK, T. H., STEINBERGER, B., SHEPHARD, G. E., DOUBROVINE, P. V., GAINA, C., DOMEIER, M., CONRAD, C. P. & SAGER, W. W. 2019. Pacific‐Panthalassic reconstructions: Overview, errata and the way forward. *Geochemistry, Geophysics, Geosystems,* 20**,** 3659-3689.

VAIL, P. R., MICHUM, R. M. & THOMPSON, S. 1977. Seismic stratigraphy and global changes of sea level. *Am. Assoc. Petroleum Geologists Mem.***,** 83-97.

VAN DER MEER, D., VAN SAPAROEA, A. V. D. B., VAN HINSBERGEN, D., VAN DE WEG, R., GODDERIS, Y., LE HIR, G. & DONNADIEU, Y. 2017. Reconstructing first-order changes in sea level during the Phanerozoic and Neoproterozoic using strontium isotopes. *Gondwana Research,* 44**,** 22-34.

VAN DER MEER, D. G., ZEEBE, R. E., VAN HINSBERGEN, D. J. J., SLUIJS, A., SPAKMAN, W. & TORSVIK, T. H. 2014. Plate tectonic controls on atmospheric CO2 levels since the Triassic. *Proceedings of the National Academy of Sciences of the United States of America,* 111**,** 4380-4385.

VAN DER VOO, R., SPAKMAN, W. & BIJWAARD, H. 1999. Mesozoic subducted slabs under Siberia. *Nature,* 397**,** 246.

844 *VÉRARD, C., HOCHARD, C., BAUMGARTNER, P. O., STAMPFLI, G. M. & LIU, M. 2015. Geodynamic evolution of*
845 *the Earth over the Phanerozoic: Plate tectonic activity and palaeoclimatic indicators. Journal of*
846 *Palaeogeography, 4, 167-188.*
847 *WEN, L. X. & ANDERSON, D. L. 1995. THE FATE OF SLABS INFERRED FROM SEISMIC TOMOGRAPHY AND 130*
848 *MILLION YEARS OF SUBDUCTION. Earth and Planetary Science Letters, 133, 185-198.*
849 *WHITTAKER, J., AFONSO, J., MASTERTON, S., MÜLLER, R., WESSEL, P., WILLIAMS, S. & SETON, M. 2015. Long-*
850 *term interaction between mid-ocean ridges and mantle plumes. Nature Geoscience, 8, 479.*
851 *WHITTAKER, J., MÜLLER, R., LEITCHENKOV, G., STAGG, H., SDROLIAS, M., GAINA, C. & GONCHAROV, A. 2007.*
852 *Major Australian-Antarctic plate reorganization at Hawaiian-Emperor bend time. Science, 318, 83-86.*
853 *YANG, T., GURNIS, M. & ZAHIROVIC, S. 2016. Slab avalanche-induced tectonics in self-consistent dynamic models.*
854 *Tectonophysics.*
855 *ZAHIROVIC, S., SETON, M. & MÜLLER, R. 2014. The Cretaceous and Cenozoic tectonic evolution of Southeast*
856 *Asia. Solid Earth, 5, 227.*
857 *ZHONG, S. & RUDOLPH, M. L. 2015. On the temporal evolution of long‐wavelength mantle structure of the Earth*
858 *since the early Paleozoic. Geochemistry, Geophysics, Geosystems, 16, 1599-1615.*
859

860